Quantifying template signatures of center-of-mass motion during walking with ankle exoskeletons

Michael C. Rosenberg[1*], Joshua L. Proctor[1,2], Katherine M. Steele[1]

[1]Department of Mechanical Engineering, University of Washington, Seattle, United States of America

[2]Department of Applied Mathematics, University of Washington, Seattle, United States of America

* Corresponding author

Email: mcrose3@emory.edu (MCR)

Abstract

Predicting ankle exoskeleton impacts on an individual's walking function, stability, and efficiency remains challenging. Characterizing how the dynamics underlying center-of-mass (COM) mechanics and energetics change with exoskeletons may improve predictions of exoskeleton responses. We evaluated changes in individual-specific COM dynamics in unimpaired adults and one individual with post-stroke hemiparesis while walking in shoes-only and with passive ankle exoskeletons. We leveraged hybrid sparse identification of nonlinear dynamics (Hybrid-SINDy) – an equation-free data-driven method for inferring nonlinear hybrid dynamics using a large library of candidate functional forms – to identify functional forms that best modelled physical mechanisms describing leg-specific COM dynamics, termed *template signatures*. Across participants, Hybrid-SINDy identified template signatures comprised of leg stiffness and resting length, similar to common spring-loaded inverted pendulum models. Rotary stiffness mechanisms were identified in only 40-50% of participants. Unimpaired template signatures did not change with ankle exoskeletons ($p > 0.13$). Conversely, post-stroke paretic leg and rotary stiffness increased by 11% with zero- and high-stiffness exoskeleton, respectively, suggesting that COM dynamics may be more sensitive to exoskeletons following neurological injury. Agreement between our automatically-identified template signatures and those found from decades of biomechanics research supports Hybrid-SINDy's potential to accelerate the discovery of mechanisms underlying impaired locomotion and assistive device responses.

Introduction

Ankle exoskeletons are prescribed and designed to improve walking function and gait mechanics [1-3]. Personalized passive and powered ankle exoskeletons have shown promise to improve walking function and muscle coordination in both unimpaired adults and individuals with neurological injuries [2, 4, 5]. However, changes in gait in response to ankle exoskeletons are highly individualized, especially following neurological injury, making customization critical to improving device efficacy. For example, in stroke survivors and children with cerebral palsy, ankle exoskeletons elicit diverse – and sometimes detrimental – impacts on gait mechanics, walking speed, step length, and the energetic cost of walking[1-4]. Capturing and characterizing these responses remains challenging and hinders clinicians and designers' abilities to customize exoskeletons to support walking function.

Despite observed changes in gait mechanics and energetics with ankle exoskeletons, little is known about how task-level mechanisms, such as the control of whole-body dynamics, impact exoskeleton responses [2, 5-8]. Specifically, controlling center-of-mass (COM) motion is known to impact gait energetics and stability, and is related to clinical metrics of walking function and speed [9-11]. Modulating COM dynamics in response to exoskeletons may, therefore, be critical to maintaining stable and efficient gait. Importantly, following neurological injuries (*e.g.,* a stroke), COM energetics are altered asymmetrically, with the paretic limb doing less work on the COM [12]. Similarly, when walking with ankle exoskeletons, stroke survivors struggle to modulate their gait in energetically efficient ways [2]. However, these experimental studies did not quantify changes in the underlying COM dynamics with exoskeletons. Even in unimpaired adults it is unclear whether individuals modulate COM dynamics similarly in response to exoskeletons. Characterizing the strategies used to modulate COM dynamics with ankle exoskeletons may provide a foundational step towards understanding responses to ankle exoskeletons.

Reduced-order representations of gait dynamics provide a foundation to quantify and understand complex exoskeleton responses [13-18]. For example, Full & Kodistchek (1999) used reduced-order representations of COM dynamics, such as the spring-loaded inverted pendulum (SLIP), to quantify strategies to achieve task-level goals including COM stabilization and perturbation responses during locomotion [16]. Such reduced-order representations, or models, of gait encode neural and biomechanical dynamics using a minimalist set of physics-based mechanisms. Specifically, common reduced-order models of COM dynamics employ a variety of mechanisms, such as the SLIP leg springs or the rigid legs of an inverted pendulum walker, describe COM accelerations during gait [10, 14, 16, 17, 19-23]. Each mechanism within a model, therefore, encodes a hypothesis about how neural and biomechanical subsystems interact to achieve task-level objectives. However

Reduced-order models of locomotion, often termed *Template* models, have provided influential insights into strategies to control COM motion to achieve stable and efficient walking. For example, inverted pendulum templates have been used to study COM energetics and the transition from walking to running [17, 19], as well as strategies for energetically-efficient COM acceleration [9, 23, 24] and lateral stabilization [10, 25]. Alternative template structures, such as the bipedal spring-loaded inverted pendulum (SLIP) and its variants further improved predictions of sagittal-plane ground reaction forces (GRFs) and revealed COM stabilization strategies across different speeds [14, 21, 22, 26, 27]. Extensions of the bipedal inverted pendulum and SLIP templates include leg damping elements, rotary springs, or curved feet. Note that each mechanism describes a unique relationship between leg kinematics and COM acceleration [20, 28]. Further, given the breadth of templates proposed for human gait, the mechanisms that best describe gait are likely individual-specific. Consequently, selecting an optimal template structure to describe an individual's gait is non-trivial, particularly following neurological injury [29].

Template models that describe COM dynamics during unimpaired gait may be useful to serve as normative archetypes, from which deviations can be used to characterize altered COM dynamics.

To emphasize the individualized nature of templates, we denote the subject-specific mechanisms that best describe COM dynamics as an individual's *template signature*. For example, differences in the template signatures in children with hemiparetic cerebral palsy differed from typically developing children and between legs, with increased stiffness in the paretic limb [29, 30]. These differences suggested that children with cerebral palsy may have reduced dynamic resources available to control COM motion during walking, providing insight into individualized strategies to accelerate the COM and their implications for walking function.

Similarly, we may expect that template signatures will reveal altered COM dynamics following other forms of neurological injury (*e.g.,* stroke) and with ankle exoskeletons. However, characterizing changes in template signatures in these contexts requires addressing a major methodological challenge: Manually identifying optimal template signatures mechanisms is a slow, *ad hoc* process that relies on first-principles knowledge of the system [20]. The candidate template signature increases combinatorially with the number of candidate mechanisms. Therefore, new methods are needed to select mechanisms rapidly and systematically from a literature-based library of candidate mechanisms.

Recent advances in data-driven modeling and machine learning provide powerful techniques to flexibly identify system dynamics from data [31-34]. **Hybrid-SINDy** (*SINDy: Sparse identification of nonlinear dynamics* [31]) identifies sparse nonlinear dynamics in hybrid systems from time-series data, making it particularly relevant to identifying template signatures of walking, which often have distinct dynamics based on foot contact configuration [29, 33]. Importantly, Hybrid-SINDy identifies a large number of candidate dynamical models (*e.g.,* template signatures) from an arbitrary library of possible functional forms (*i.e.,* mechanisms). The algorithm uses information criteria to determine levels of support for each candidate model and selects only those that are parsimonious *and* highly representative of the system [35]. Consequently, this approach enables rapid, systematic identification of individual-specific template signatures while leveraging first-principles knowledge of the physics of human gait.

The purpose of this study was to identify changes in template signatures in response to ankle exoskeletons and evaluate how neurological injuries may alter template signatures in response to exoskeletons. We used the Hybrid-SINDy algorithm to identify template signatures that encode COM dynamics during walking in unimpaired adults and how those signatures changed with hinged and stiff ankle exoskeletons. We hypothesized that ankle exoskeletons would primarily increase leg stiffness. Additionally, to examine the potential of template signatures to encode changes in COM dynamics for individuals with neurological injuries, we present a case study evaluating altered template signatures in an individual with post-stroke hemiparesis. To our knowledge, this work is the first to employ physics-informed data-driven modeling techniques to select low-dimensional, interpretable, representations of walking dynamics with ankle exoskeletons.

Methods

Data collection

We collected 3D marker trajectories using a ten-camera motion capture system (Qualisys AB, Gothenburg, SE) and ground reaction forces (GRFs) using an instrumented treadmill (Bertec Inc., Columbus, USA) in twelve unimpaired adults (6M/6F; age = 23.9 ± 1.8 years; height = 1.69 ± 0.10 m; mass = 66.5 ± 11.7 kg) and one stroke survivor with lower-limb hemiparesis (*sex not disclosed*; age = 24 years; height = 1.70 m; mass = 68.0 kg). Participants walked on a treadmill in shoes-only and with bilateral passive ankle exoskeletons under two conditions: zero resistance to ankle flexion (*i.e.,* zero stiffness; K_0) and high dorsiflexion resistance (*i.e.,* high stiffness; K_H = 5.1 Nm/deg; Figure 1). A detailed description of the experimental protocol and data preprocessing can be found in [36]. Briefly, in a second session following a practice session, data were collected while participants walked at their self-selected speed for four minutes per condition. To mitigate fatigue, the post-stroke participant walked under the same protocol, but for only three minutes per condition [37]. This study was approved by the University of Washington Institutional Review Board (#47744) and all participants provided written informed consent to participate in the study.

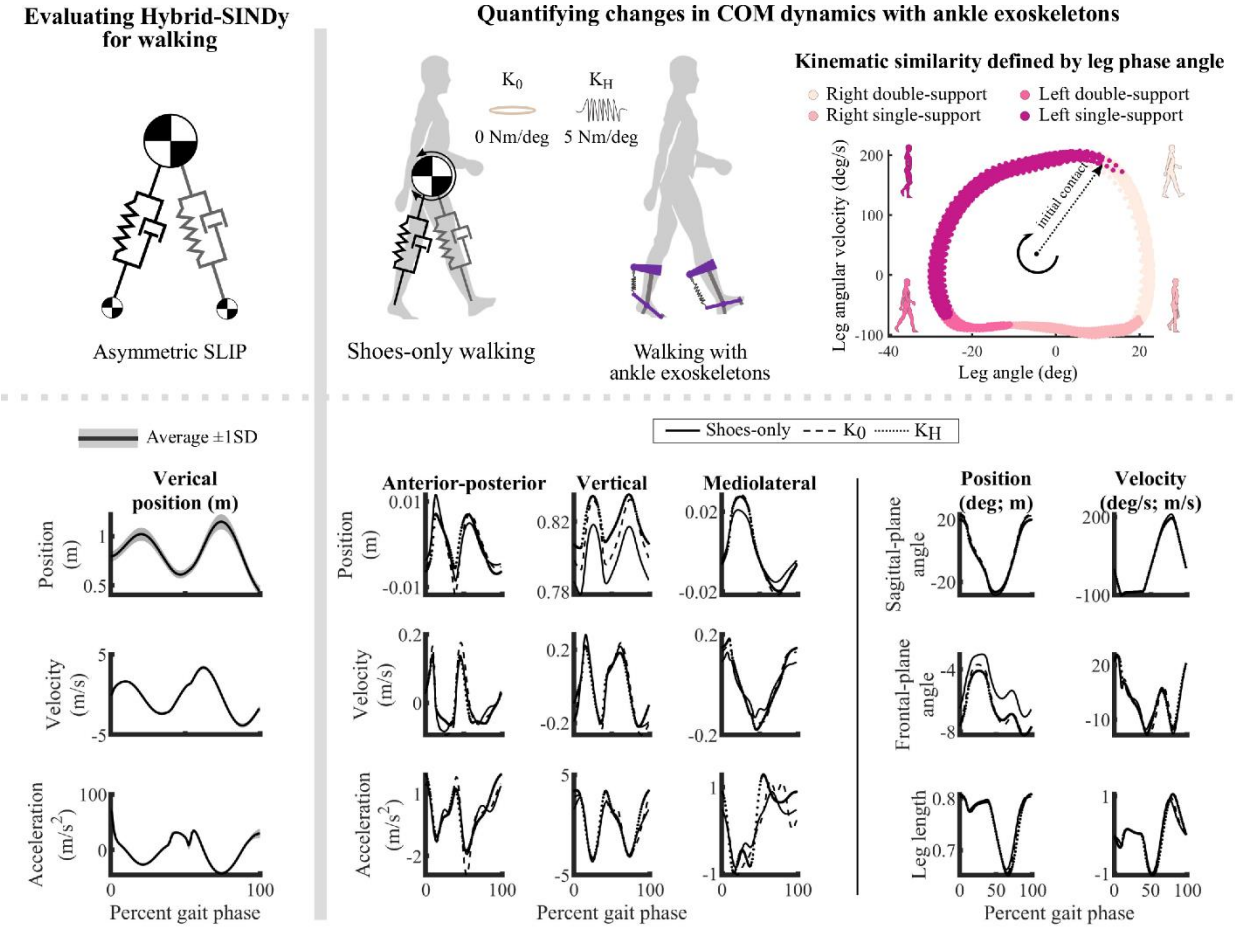

Figure 1 – Top: Two-dimensional depictions of the simulated SLIP (left) and human walking (right). The simulated SLIP used leg springs and dampers, as well as foot masses to simulate full strides. Participants walked on a treadmill in shoes-only and in ankle exoskeletons under zero- (K_0) and high-stiffness (K_H) conditions. The pink phase portrait was used to define a kinematic phase variable for clustering similar measurements. Colors denote gait phases corresponding to first and second double-limb support, single-limb support, and swing. Bottom: Time-series measurements of COM position, velocity, and acceleration for the simulated SLIP (left; average ± 1SD) and an exemplary unimpaired adult participant (right). For human walking, 3D COM states (middle) and leg states (right) are shown for the three exoskeleton conditions. The leg length and velocity, and sagittal- and frontal-plane leg angles determined leg forcing, while COM position determined the direction of forcing.

Estimating template signatures with Hybrid-SINDy

To identify mechanisms describing COM acceleration, we used the Hybrid-SINDy algorithm to identify template signatures with and without ankle exoskeletons. Note that, for each exoskeleton condition, we used OpenSim's *Body Kinematics* algorithm to estimate the COM and foot positions [38, 39]. In this

146 section, we describe the SINDy and Hybrid-SINDy algorithms in the context identifying template
147 signatures, while more detailed explanations can be found in [31] and [33, 34]. Let 3D COM
148 accelerations, $\ddot{\boldsymbol{q}}(t) \in \mathbb{R}^{m\times n}$, be described by continuous-time nonlinear dynamics, $f\big(q(t), \dot{q}(t)\big)$, where
149 m denotes the number of samples and n=3 output:

$$\frac{d^2}{dt^2}\boldsymbol{q}(t) = \ddot{\boldsymbol{q}}(t) = f\big(\boldsymbol{q}(t), \dot{\boldsymbol{q}}(t)\big), \quad (1)$$

150 where time is denoted by $t \in \mathbb{R}^{m\times 1}$, and $q(t)$ and $\dot{q}(t)$ represent COM positions and velocities relative to
151 the feet, respectively, in $\mathbb{R}^{m\times n}$, in the anterior-posterior, vertical, and mediolateral directions. We assume
152 that only a small number of functional forms (*i.e.,* mechanisms) in $f(q(t), \dot{q}(t))$ describe most of the
153 system's behavior. We omit the time notation in the remaining sections.
154

155 ## Sparse Identification of Nonlinear Dynamics (SINDy)

156 The SINDy algorithm ([31]) recovers sparse nonlinear dynamics from a library of candidate functional
157 forms, which may consist of arbitrary nonlinear functions of system measurements. Adopting the notation
158 from [33], we can rewrite the dynamics in equation 1 as:

$$\ddot{\boldsymbol{q}} = \boldsymbol{\Theta}(\boldsymbol{q}, \dot{\boldsymbol{q}})\boldsymbol{\Xi}, \quad (2)$$

159 where $\Xi \in \mathbb{R}^{p\times n}$, is a linear map from nonlinear function library encoding mechanisms potentially
160 describing COM accelerations, $\boldsymbol{\Theta}(\boldsymbol{q}, \dot{\boldsymbol{q}}) \in \mathbb{R}^{m\times p}$, to COM accelerations, $\ddot{\boldsymbol{q}}$. The coefficients in Ξ,
161 therefore, represent template signatures parameters, while $\boldsymbol{\Theta}$ encodes template signature structure. We
162 included $p = 14$ functional forms in the function library, described below. The SINDy algorithm
163 promotes sparsity using sequential least-squares regression with hard thresholding, with the threshold
164 defined by the sparsity parameter, λ (Eq 3) [33, 34]. This thresholding approach penalizes the zero-norm
165 of Ξ and solves:

$$\min_{\Xi} || \boldsymbol{\Theta}(\boldsymbol{q}, \dot{\boldsymbol{q}})\boldsymbol{\Xi} - \ddot{\boldsymbol{q}}||_2 + \lambda\|\boldsymbol{\Xi}\|_0, \quad (3)$$

166

Hybrid-SINDy

Hybrid-SINDy extends SINDy in two important ways. First, Hybrid-SINDy uses clustering to generalize SINDy to hybrid systems. For human walking data clustering, enables unique dynamics to be identified in each hybrid regime, such as those defined by contact configuration (*i.e.,* single- and double-limb support) [11, 15, 19]. Second, Hybrid-SINDy uses information criteria to automatically select the system dynamics that best describe the data. This approach enables competing hypotheses about the mechanisms describing COM acceleration to be rapidly and systematically compared, thereby highlighting mechanisms that are common across individuals and those unique to a subset of individuals.

Applying Hybrid-SINDy to walking

We applied the Hybrid-SINDy algorithm to human gait using the following steps for each participant and walking condition (Figure 2). Note that within each hybrid regime of the gait cycle, we expanded upon the original Hybrid-SINDy algorithm by using multi-model inference to define a single template signature when multiple signatures were plausible (Step 5) [33, 34].

1. *Clustering*: For each sample in the training set, we generated cluster the samples' 800 nearest neighbors and identified the centroid of each cluster. The average cluster width (7.4% of a stride) was less than double-limb support. We used the right leg angle and angular velocity with respect to vertical as our clustering parameters [36].
2. *Model estimation*: For each cluster, we used SINDy to identify multiple template signatures, by sweeping 40 sparsity threshold values, typically producing 5-15 unique signatures per cluster.
3. *Model evaluation and selection*: Using held-out data, we evaluated the ability of each template signature to reconstruct COM accelerations in the anterior-posterior, vertical, and mediolateral directions. We computed the average reconstruction error of held-out data over gait phases, ϕ, spanning 0-100% of a stride (Eq 4).

$$\text{error}_{\phi} = |\boldsymbol{\Theta}(\boldsymbol{q}, \dot{\boldsymbol{q}})\boldsymbol{\Xi} - \ddot{\mathbf{q}}|_{\phi}$$

We selected template signatures based on two criteria: First, we discarded signatures that were identified in less than 1% of training clusters. Frequently occurring template signatures are more likely to be robust to measurement noise or stride-to-stride variability, making them better representations of an individual's gait dynamics [33].

Second, for each hybrid regime – single- and double-limb support – we selected the frequently occurring template signatures that had the highest likelihood of being the correct signature describing COM accelerations according to the Akaike Information Criterion (AIC) [35, 40]. The AIC is widely used to compare candidate representations of system dynamics (*e.g.,* template signatures) according to their number of free parameters and log-likelihood [35]. The AIC favors parsimonious, highly-representative models, which is ideal for identifying minimalist representations of gait dynamics. Like Mangan and colleagues, we used the AIC corrected for finite sample sizes (AICc) and compared signatures according to their relative AICc score ($\Delta_j = AICc_j - AICc_{min}$ for signature j) [33, 35]. The best model according to the relative AICc score has a score of $\Delta_j = 0$ and all other models had higher scores. Burnham and Anderson noted that models with $\Delta_j \leq 2$ have substantial support, while $\Delta_j > 7$ have low support [35]. We adopted the threshold of [33], deeming template signatures with $\Delta_j \leq 3$ to be *plausible*.

4. *Multi-model inference*: Since human gait dynamics are not strictly hybrid, multiple template signatures are likely to be deemed plausible in each hybrid regime. To construct a single template signature for each hybrid gait regime, we computed a weighted-average signature using Akaike weights, ω_j, where j is the j^{th} plausible model in a hybrid regime [35]. Akaike weights are

$$\omega_j = \frac{\exp\left(-\frac{\Delta_j}{2}\right)}{\sum_{r=1}^{R} \exp\left(-\frac{\Delta_r}{2}\right)}, \quad (5)$$

where $\exp\left(-\frac{\Delta_j}{2}\right)$ defines the likelihood of the j^{th} template signature given the observations [35]. This approach weights each signature based on its likelihood relative to the other plausible signatures.

5. *Uncertainty estimation*: To evaluate the robustness of the template signatures to noise and stride-to-stride variations in the data, we performed 200 bootstrapped estimates of template signatures parameters using the data in the corresponding hybrid regimes. The template signatures were characterized by the mean and standard deviation of the bootstrapped parameters.

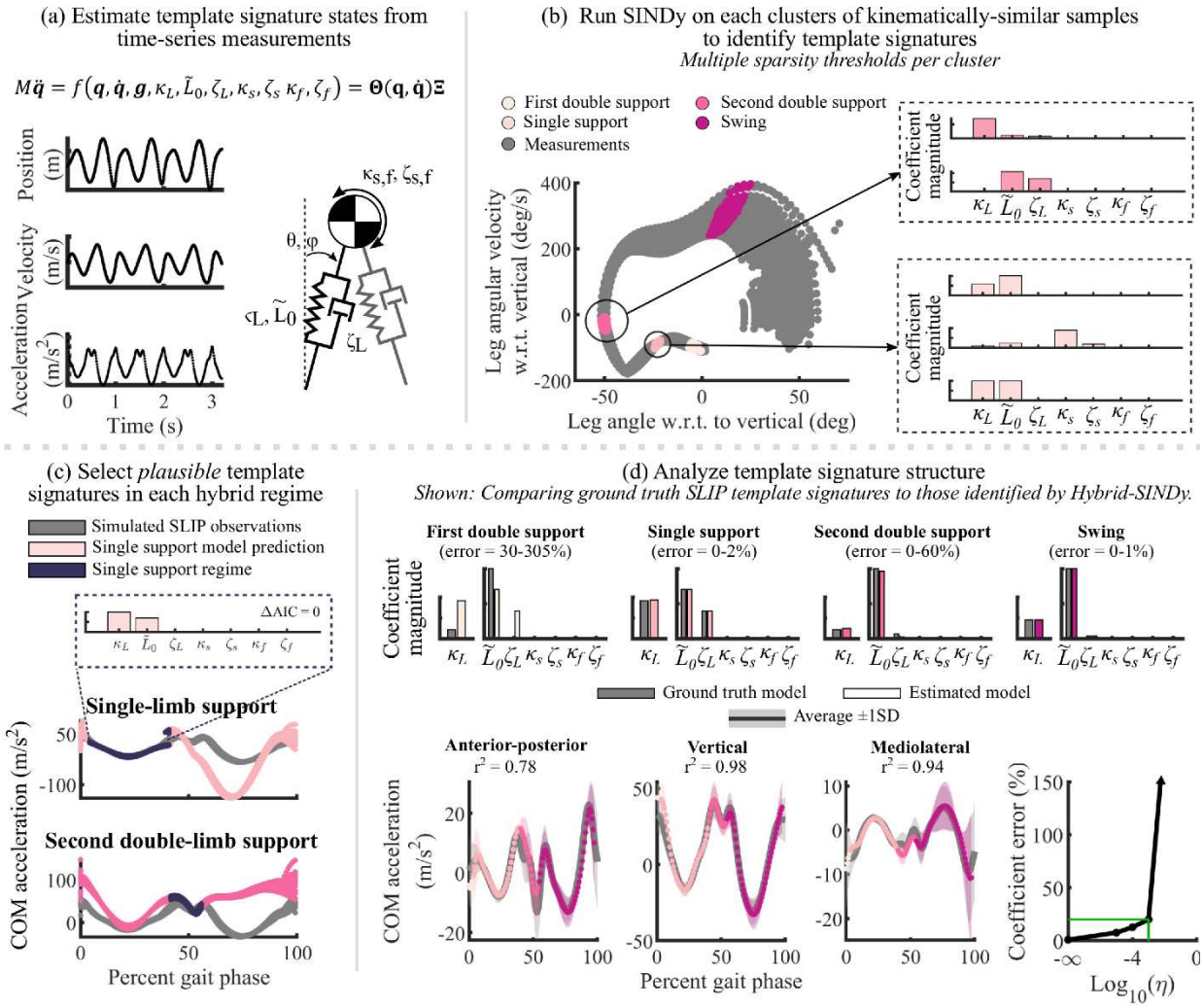

Figure 2 – The Hybrid-SINDy algorithm, applied to a simulated 3D-SLIP walking model. (a) COM and foot measurements from the simulated SLIP were used to approximate nonlinear SLIP states, $\boldsymbol{\Theta(q, \dot{q})}$, as shown in the equation and the SLIP diagram. Variables can be found in Table 1. (b) Kinematically-similar measurements were used to cluster the data (gray) and exemplary template signature parameters from two clusters. For each cluster, multiple signatures of different complexities

were identified. (c) Each signature was evaluated in the hybrid regime containing the cluster centroid. The plots show COM accelerations and predictions in single-limb (top) and second double-limb (bottom) support. Error is low only in the correct hybrid regime for each signature (purple). (d) Top: Ground-truth (gray) and identified (colors) template signatures in each hybrid regime, with percent errors compared to ground-truth. Bottom: Average (±1SD) observed (gray) and predicted (colors) COM accelerations. Colors denote each hybrid regime. The rightmost plot shows the average percent error in template signature coefficients during single-limb support and swing with increasing measurement noise (η). Green lines denote the approximate noise level of marker-based motion capture.

Template signatures mechanisms and dynamics

To model three-dimensional COM dynamics during walking, we created a function library of the following candidate mechanisms based on prior literature (Table 1):

- *Rigid legs*, which reflected pendular gait in stance [10, 13, 15, 19, 24]. Pendular gait is energetically passive and reflects kinetic and potential energy transfer during walking but cannot explain GRFs and lacks double-limb support phase [15, 22, 41].
- *Leg springs* ([14, 20-22, 26]) and *dampers* ([28]), which produce force along the leg. Leg springs are common energetically-conservative mechanisms used to describe walking and running dynamics, and enable a double-limb support phase. Leg dampers are less common, but have been used to capture non-conservative gait dynamics [28].
- *Rotary springs* ([14, 20]) and *dampers* in the sagittal and frontal planes, which enable forcing transverse to the leg axis. The addition of a rotary springs has been show to improve reconstructions of anterior-posterior GRFs in a bipedal SLIP [20]. We did not identify rotary damping elements in prior literature but include them as a candidate mechanism describing non-conservative transverse forcing.

The mechanisms selected by the Hybrid-SINDy algorithm define the template signature *structure*, which describes characteristic strategies to accelerate the COM. The identified signature *parameters* describe each mechanism's contribution to COM accelerations.

The dynamics of a three-dimensional bipedal SLIP augmented with damping and rotary mechanisms may be written as

$$M(\ddot{\boldsymbol{q}} - \boldsymbol{g}) = \sum_{j=R,L} \left(-\left[k_L(L - L_0) + c\dot{L}\right]\frac{\boldsymbol{q}}{L} - \left[k_s\theta + c_s\dot{\theta}\right]\frac{\boldsymbol{q}}{L_s^2} - \left[k_f\phi + c_f\dot{\phi}\right]\frac{\boldsymbol{q}}{L_f^2} \right)_j, \qquad 6$$

where M is body mass, $\boldsymbol{g}$ is the gravity vector, ϕ describes the traverse-plane leg angle, and θ describes the leg angle from vertical in the direction defined by ϕ [20, 26]. The summation represents total force generated by the legs on the COM. The left-most brackets contain mechanisms that impart forces radially along the leg: k_L is the leg stiffness, L is the instantaneous leg length, L_0 is the leg resting length, c_L is the leg damping, $\dot{L}$ is the instantaneous leg velocity. We henceforth denote L_0 as *leg length* for clarity. The middle bracket contains mechanisms that impart forces transverse to the leg axis in the sagittal plane: k_s and c_s are the sagittal-plane rotary stiffness and damping, respectively. L_s denotes the sagittal-plane leg projection. Analogously in the right-most brackets, k_f and c_f represent the frontal-plane rotary stiffness and damping, respectively, and L_f denotes the frontal-plane leg projection.

Normalized template mechanisms

To account for inter-individual differences in walking speed and body size during analysis, we normalized the template signatures during analysis (Table 1). Leg stiffness was normalized as in [18, 20, 33]. Leg resting length normalized to the measured leg length [20, 28]. Rotary stiffness was normalized according to [20]. All damping terms were converted to damping ratios [28]. The normalized leg, sagittal-plane, and frontal-plane stiffness mechanisms are denoted by κ_L, κ_s, and κ_f, respectively. The normalized leg, sagittal-plane, and frontal-plane damping mechanisms are denoted by ζ_L, ζ_s, and ζ, respectively. Normalized leg length is denoted $\tilde{L}_0$. We can rewrite equation 6 as a linear combination of our normalized coefficients and nonlinear transformations of our states:

$$M(\ddot{\boldsymbol{q}} - \boldsymbol{g}) = \begin{bmatrix} \kappa_L & \kappa_L\tilde{L}_0 & \zeta_L & \kappa_s & \zeta_s & \kappa_f & \zeta_f \end{bmatrix}_j \boldsymbol{\Theta}(\boldsymbol{q}, \dot{\boldsymbol{q}}), \quad j = \{R, L\} \qquad 7$$

The COM position and velocity relative to the feet were used to compute candidate template signature states: leg lengths and lengthening velocities, sagittal-plane leg angles and angular velocities relative to vertical, and frontal-plane leg angles and angular velocities relative to vertical.

Table 1 – List of template signature terms.

Term	Symbol	Normalized form
Leg stiffness	κ_L	$\frac{k_L L_{bio}}{Mg}$
Leg resting length	$\tilde{L}_0$	L_0/L_{bio}
Leg damping	ζ_L	$\frac{c_L}{2\sqrt{k_L M}}$
Sagittal-plane rotary stiffness	κ_s	$\frac{k_s}{MgL_{bio}}$
Sagittal-plane rotary damping	ζ_s	$\frac{c_s}{\sqrt{\kappa_s M L_{bio}^2}}$
Frontal-plane rotary stiffness	κ_f	$\frac{k_f}{MgL_{bio}}$
Frontal-plane rotary damping	ζ_f	$\frac{c_f}{\sqrt{\kappa_f M L_{bio}^2}}$

c_L=leg damping; c_s=sagittal-plane rotary damping; c_f=sagittal-plane rotary damping; g = gravitational acceleration; k_L=leg stiffness; k_s=sagittal-plane rotary stiffness; k_f=sagittal-plane rotary stiffness; L_{bio} biological leg length; M = body mass

Evaluating Hybrid-SINDy's ability to select template signatures

To evaluate Hybrid-SINDy's ability to accurately identify and select walking dynamics, we evaluated the algorithm on surrogate data of a simulated bipedal SLIP walker with known dynamics (Figure 1 & Figure 2) [26]. The bipedal SLIP had asymmetric leg stiffness and damping, and masses representing the pelvis (M = 56 kg) and feet (M_f = 7 kg) to simulate a full gait cycle (Table 2). We omitted rotary mechanisms from the SLIP dynamics but used the full function library described in equation 6. We simulated 120 gait cycles from randomly perturbed initial conditions with an average initial velocity of 1.20 m/s. As

SINDy's performance is sensitive to sensor noise, we identified template signatures using simulation measurements with added Gaussian noise ranging logarithmically from 10 nm to 10 cm applied to the position measurements [31]. We quantified the Hybrid-SINDy's ability to reconstruct model dynamics using the number of correctly-selected mechanisms and the accuracy of estimated coefficients.

Table 2 – Bipedal SLIP normalized simulation parameters.

Term	*[Right leg, Left leg]*			
	DS_1	**SS**	**DS_2**	**SW**
κ_L	[10.8, 9.1]	[25.1, 18.82]	[9.03, 10.68]	[36.6,25.3]
$\tilde{L}_0$	[1.0, 1.0]	[1.0, 0.7]	[1.0, 1.0]	[0.7, 0.7]
ζ_L	[0.04, -0.07]	[-0.03, -0.04]	[0, 0]	[-0.40, -0.57]
κ_s	0	0	0	0
ζ_s	0	0	0	0
κ_f	0	0	0	0
ζ_f	0	0	0	0

Identifying template signatures in human gait

We estimated unique template signatures that predicted COM accelerations using the Hybrid-SINDy algorithm for each participant and ankle exoskeleton condition. We used 10800 samples (90 seconds) were available for clustering and we identified template signatures for the first 3600 samples. An additional 3600 samples of held-out data were used for model evaluation and selection.

To evaluate the extent to which each mechanism described COM accelerations in unimpaired adults, we analyzed the proportion of participants for whom each template signature coefficient was selected. Signature terms are identified across individuals represent mechanisms fundamental to COM dynamics, while infrequently identified mechanisms describe individual-specific features of COM dynamics.

To determine if unimpaired COM dynamics during shoes-only walking generalized to walking with ankle exoskeletons, we evaluated the ability of shoe-walking template signature structures to reconstruct COM accelerations in the K_0 and K_H conditions. We used least-squares regression to identify template signature parameters for the K_0 and K_H conditions using the shoes-only template signature structure. We compared the relative AICc ($\Delta AICc$) scores between these signature structures and those of the signature structures specific to the K_0 and K_H trials. We used one-sample paired t-tests ($\alpha = 0.05$) to determine if shoes-only template signatures were less plausible (*i.e.,* $\Delta AICc \geq 3$) than signature structures selected for the K_0 and K_H conditions.

To determine the frame and mass of the ankle exoskeletons impacted COM dynamics, we compared template signature coefficients between the K_0 and Shoe conditions. Similarly, to evaluate the impacts of exoskeleton stiffness on COM dynamics, we compared template signature coefficients in the K_H and K_0 conditions. For both comparisons, we used paired two-sample t-tests with Holm-Sidak step-down corrections for multiple comparisons ($\alpha = 0.05$) [42]. Because we found that shoes-only template signature structures were plausible for most unimpaired participants, we used the shoes-only template signatures structure to estimate signature coefficients in all exoskeleton conditions.

To determine if COM dynamics may be altered post-stroke, we first computed the percent difference in the non-paretic and paretic limb template signature parameters during shoes-only walking in one individual with post-stroke hemiparesis. We also evaluated changes in post-stroke COM dynamics with ankle exoskeletons by computing percent changes in template signature coefficients for the K_0 condition compared to the shoes-only and K_H conditions.

Results

Hybrid-SINDy identified COM dynamics of a simulated SLIP

The Hybrid-SINDy algorithm correctly identified the salient features of the simulated SLIP's template signature during single-limb support (Figure 2). Specifically, Hybrid-SINDy identified non-zero leg stiffness (κ_L), resting length ($\tilde{L}$), and damping (ζ_L) terms only – consistent with the SLIP's dynamics. In the noise-free condition, 86% of terms were correctly selected and only one term, leg damping in first double-limb support, was incorrectly selected. Both double-limb support regimes were very short in the simulated SLIP: 1.3% and 4.6% of samples in first and second double-limb support – smaller than the 7.4% of the training data in each cluster. Consequently, all clusters with centroids in the double-limb support regimes contained samples spanning double- and single-limb support. Hybrid-SINDy incorrectly omitted only damping terms with small coefficients (Table 2). Without measurement noise, in single-limb support and swing, coefficients were within 2% of the ground truth values. When measurement noise with a standard deviation of 1 mm – similar to that of our motion capture system – was added to the system measurements, Hybrid-SINDy correctly selected only 63% of mechanisms, though incorrect mechanisms selection occurred primarily in double-limb support. Template signature coefficients were estimated with an average error of less than 29% in single-limb support and swing (Figure 2). In single-limb support, Hybrid-SINDy was still able to estimate large coefficients (*i.e.,* leg stiffness and resting length) with less than 1% error.

Shoes-only template signatures revealed common and subject-specific COM mechanisms

When walking in shoes-only, SLIP-like template signatures best described COM dynamics across unimpaired participants. In both double-limb and single-limb support, SLIP mechanisms – leg stiffness and leg length – were selected in 96-100% of limbs (Figure 3). Unimpaired template signatures were not significantly different between legs (paired 2-sample t-test; $p > 0.01$). However, template signatures varied during double-limb support: Rotary stiffness terms were selected in 58-67% of limbs in the first

342 double-limb support and 83-95% of limbs during second double-limb support. Except for sagittal-plane
343 damping, damping terms were selected in less than 20% of limbs. As expected during swing, when the
344 limb should not contribute to COM accelerations, no terms were selected. We omit the swing regime from
345 remaining analyses.
346

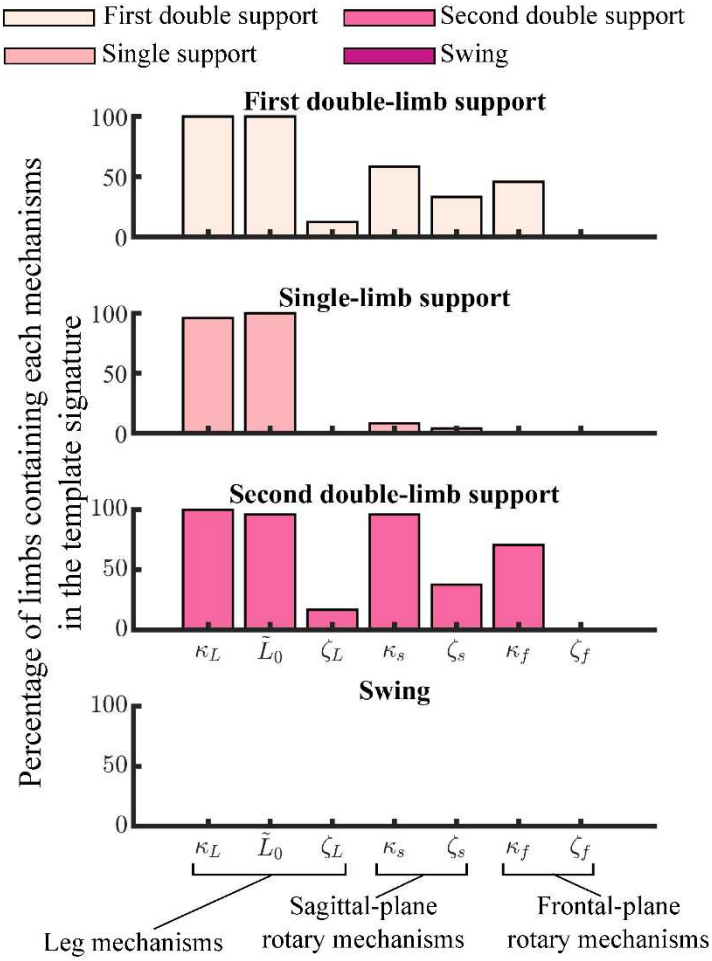

Figure 3 – The percentage of unimpaired limbs (24 limbs) whose template signatures contained each mechanism in each hybrid regime. Colors denote each hybrid regime. Mechanisms selected in a larger percentage of legs suggest common representations of COM dynamics, while less frequently-selected mechanisms reflect individual-specific features describing COM dynamics.

347

348 For each participant, template signatures were robust to stride-to-stride variations during single-limb
349 support: stiffness and leg length exhibited coefficients of variation (CVs) less than 0.021 ± 0.015. In both

double-limb support phases, CVs of stiffness and sagittal-plane rotary damping ranged from 0.11 – 0.26. Less frequently selected mechanisms in double-limb support – leg damping and frontal-plane damping – were highly variable, with CVs ranging from 0.082 – 0.442.

Across unimpaired participants, single-limb support leg length was most consistent (CV = 0.03), while leg stiffness was more variable (CV = 0.28; Figure 4; top). However, interindividual variability in double-limb support leg and rotary stiffness was larger (CV = 0.43 – 1.94). Despite this variability, template signatures reconstructed participants' COM accelerations well, 32-85% of the variance in 3D COM accelerations (Figure 4; bottom).

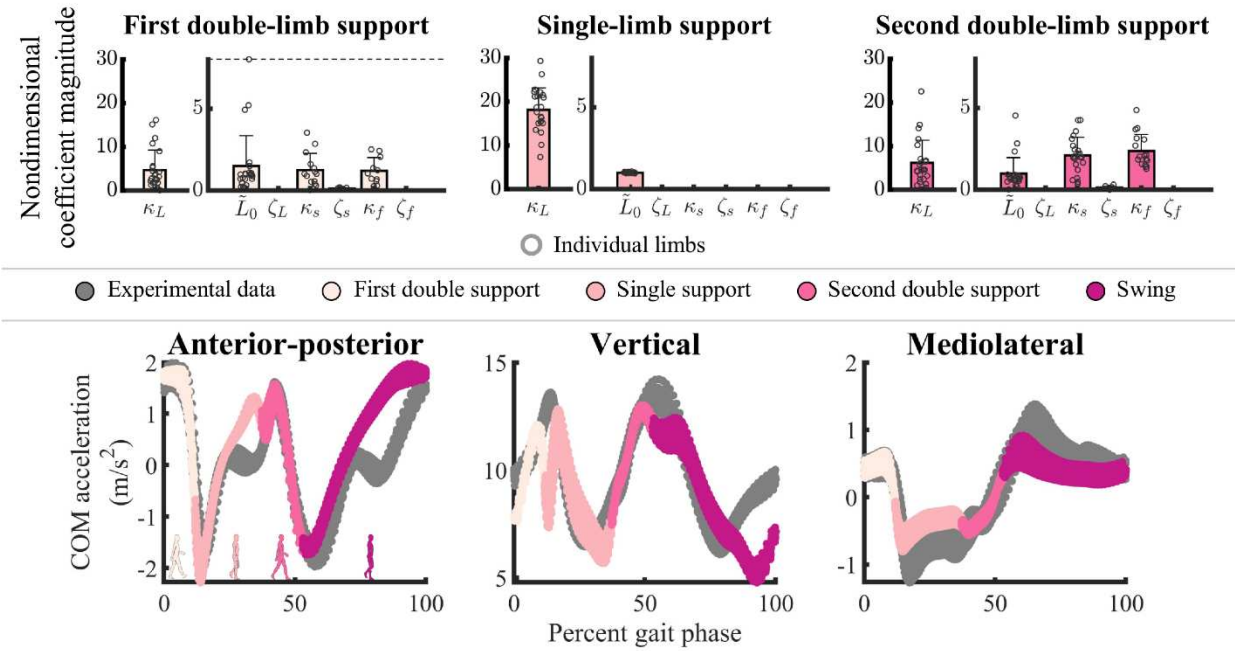

Figure 4 – Normalized template signatures (top) and reconstructed COM accelerations (bottom) for shoes-only walking in each hybrid regime. Top: Bars denote the average template signature (+1SD) in single- and double-limb support. The small circles represent individual limbs. Note that we omitted mechanisms that were selected in less than 25% of participants. The dashed lines truncate large terms for clarity. Bottom: Experimental and predicted COM accelerations from the test dataset of an exemplary unimpaired participant. The gray dots denote the experimental accelerations, while the colors correspond to predictions in each hybrid regime.

Ankle exoskeleton impacts on unimpaired COM dynamics were small

The shoes-only template signature structures reconstructed K_0 and K_H COM dynamics with similar accuracy to the K_0 ($\Delta AICc = 0.2 \pm 0.7$; p = 0.93) and K_H ($\Delta AICc = 0.7 \pm 2.9$; p = 0.24) signature structures, respectively, in single-limb support. Conversely, in double-limb support, shoes-only signatures did not consistently reconstruct K_0 or K_H COM dynamics, with relative AICc scores ranging from $-118 \leq \Delta AICc < 220$ (Figure 5; top). The negative relative AICc scores occurred when the shoes-only template signature structure was never identified by Hybrid-SINDy in the exoskeleton conditions. Therefore, to compare signature coefficients between exoskeleton conditions, we constrained each participant's template signatures to that selected in the shoes-only condition.

Using this approach, we found that no unimpaired template signature coefficients changed significantly when walking in shoes-only, zero-stiffness exoskeletons (K_0), and stiff exoskeletons (K_H) ($p > 0.05$). Specific to our hypothesis, we found that neither ankle exoskeleton mass and frame (K_0) nor stiffness (K_H) had a significant impact on leg stiffness in any gait phase ($p > 0.13$) (Figure 5; bottom).

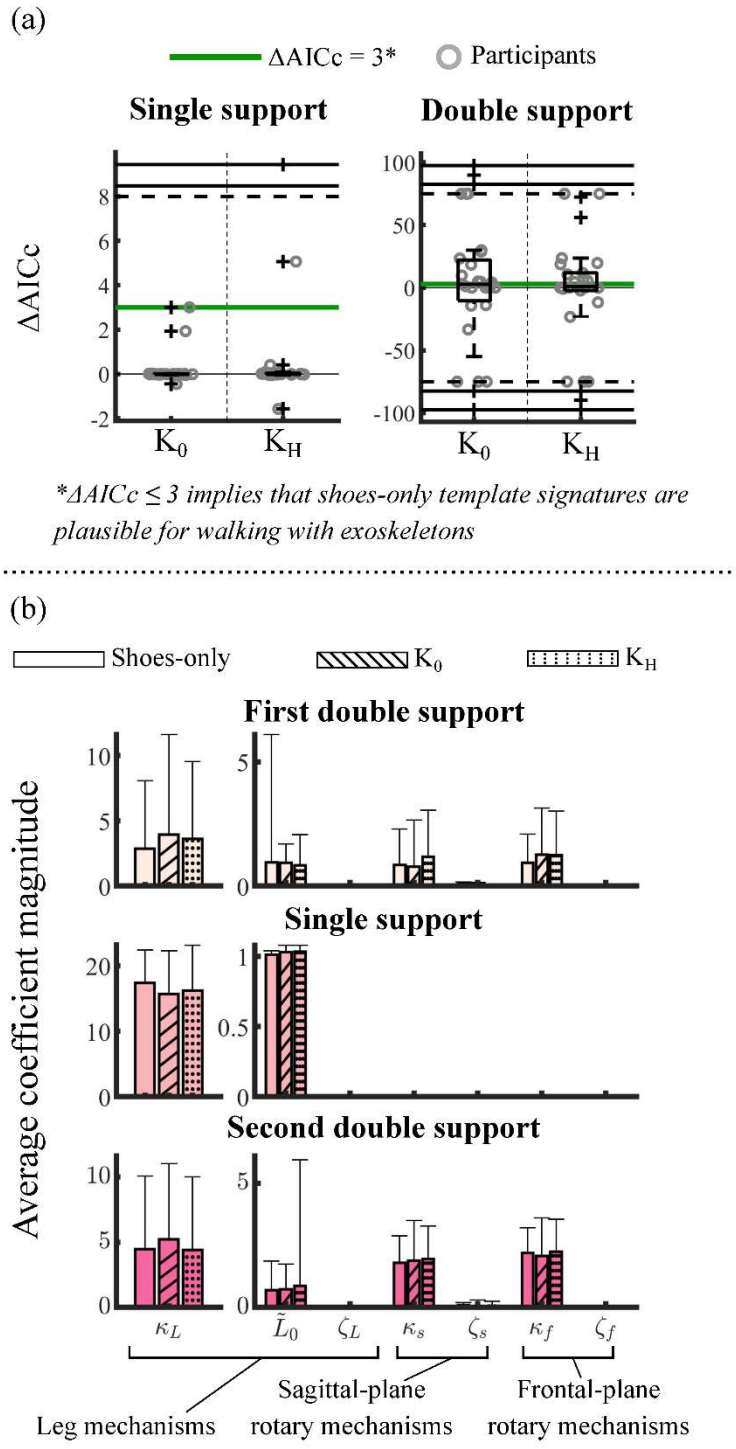

Figure 5 – (a) Relative AICc ($\Delta AICc$) between template signatures identified specifically for the K_0 and K_H conditions, and signatures constrained to the shoes-only signature structures. Positive $\Delta AICc$ values indicate that shoes-only signature structures were less plausible than those identified specifically for each condition. $\Delta AICc$ scores are shown for single-limb support (left) and double-limb support (right). $\Delta AICc \leq 3$ (green lines) denote plausible shoe template signature structures. For double-limb support,

large $\Delta AICc$ scores are truncated at $\Delta AICc = \pm 75$ for clarity. (b) Template signatures of walking in shoes only (solid bars), zero-stiffness (K_0; slashed bars) exoskeletons, and high-stiffness exoskeletons (K_H; dotted bars) during single- and double-limb support. Bars represent the average (+1SD) template signature across participants. Leg stiffness (κ_L) is included on a separate subplot for clarity. The large variability in leg length during double-limb support is due one limb with a high resting length.

Template signatures reveal altered COM dynamics post-stroke

During shoes-only walking, the stroke survivor's template signature revealed distinct strategies for accelerating the COM in double, but not single-limb support. The template signature structure was symmetric between the paretic and non-paretic limbs during single-limb support, consisting of only leg stiffness and resting length (Figure 6). However, the paretic limb was 31% stiffer than the non-paretic limb. Conversely, template signature structure differed in double-limb support, with rotary stiffness mechanisms improving descriptions of COM dynamics in only the paretic limb. During first double-limb support, leg damping and rotary stiffness were selected in only the paretic limb. In second double-limb support, both paretic and non-paretic rotary stiffness mechanisms were selected. Due to asymmetric template signature structures, we did not compare signature coefficients in double-limb support.

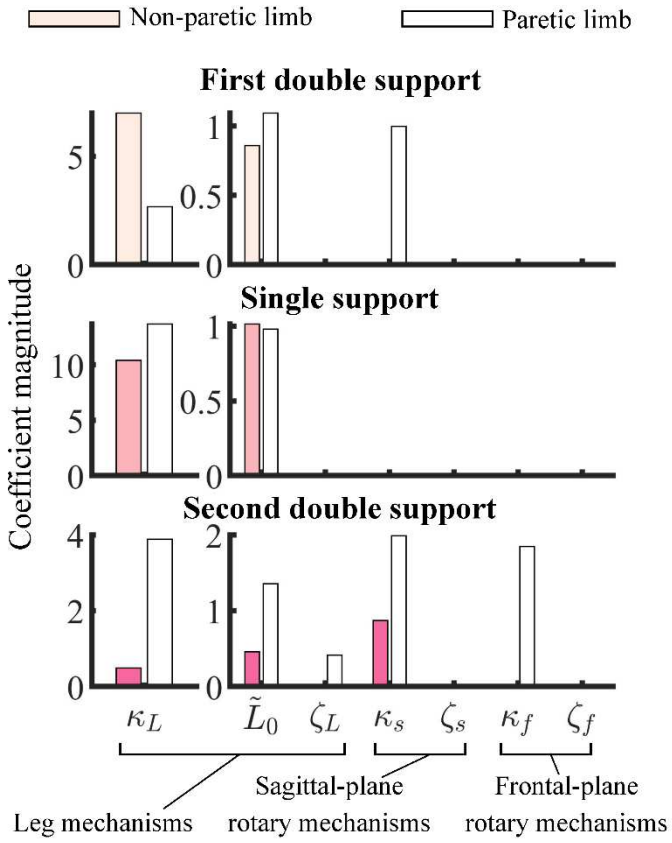

Figure 6 – Non-paretic (colored bars) and paretic (white bars) template signatures for one individual with post-stroke hemiparesis. This participant's template signatures differed in the paretic and non-paretic limbs in double-limb support, as shown by the zero-values for non-paretic sagittal-plane rotary stiffness in first double-limb support (top row) and the leg damping and frontal-plane stiffness in double-limb support (third row).

Ankle exoskeletons impacted post-stroke COM dynamics

The exoskeleton mass and frame (Shoe vs. K_0) primarily impacted the stroke survivor's paretic leg stiffness and non-paretic leg rotary stiffness. Compared to walking in shoes-only, paretic leg stiffness was 11% greater in the zero-stiffness (K_0) exoskeleton condition in single-limb support and over twice as stiff in double-limb support (Figure 7; slashed bars). Responses to the K_0 exoskeleton condition were asymmetric, with the non-paretic leg being slightly (3%) less stiff in the K_0 condition than the shoes-only

393 condition in single-limb support, while sagittal-plane stiffness was 41% larger in second double-limb
394 support. Conversely, exoskeleton stiffness (K_0 vs. K_H) had small impacts on paretic-leg template
395 signatures. In the high-stiffness (K_H) exoskeleton condition, single-limb support paretic leg stiffness was
396 only 1% larger than in the K_0 condition (Figure 7; dotted bars). Both paretic and non-paretic leg rotary
397 stiffness were 11% greater in second double limb support than in the K_0 condition. Non-paretic leg
398 stiffness was 49% smaller than with zero-stiffness (K_0) exoskeletons in single-limb support.
399

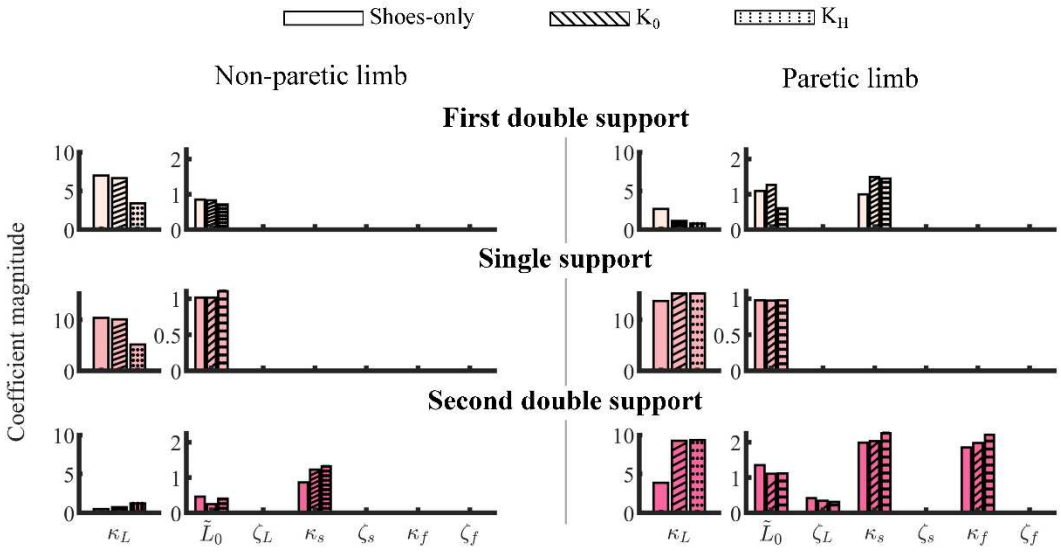

Figure 7 – Template signatures of a stroke survivor walking in the shoes-only (clear bars), zero-stiffness (K_0; slashed bars), and high-stiffness (K_H; dotted bars) ankle exoskeleton conditions for the non-paretic (left) and paretic (right) limbs. Bars represent the average template signatures over 200 bootstrapped model fitting iterations. Colors correspond to each hybrid regime.

400

Discussion

Template signatures elucidate exoskeleton impacts on COM dynamics

We evaluated the impacts of passive ankle exoskeletons on subject-specific COM dynamics – described by template signatures – using a recently-developed data-driven modeling framework, Hybrid-SINDy. To our knowledge, this is the first study to quantitatively characterize the impacts of ankle exoskeletons on COM dynamics. We used simulated SLIP to show that Hybrid-SINDy was robust to measurement noise comparable to marker-based motion capture ($\eta = 1\ mm$). Therefore, template signature structure and parameters identified by Hybrid-SINDy for human walking likely encode meaningful information about COM dynamics. Contrary to our hypothesis, leg stiffness did not change in response to the ankle exoskeletons in unimpaired adults. Further, template signatures identified from shoe walking were plausible representations of COM dynamics when walking with ankle exoskeletons. These results suggest that unimpaired strategies to accelerate the COM during walking are minimally impacted by passive ankle exoskeletons, despite changes in kinematics and muscle activity [36]. Similarly, Collins and colleagues (2015) observed small changes in total COM power with passive ankle exoskeletons compared to walking in shoes-only, but larger changes in biological contributions to COM power [5]. However, the authors did not explain how changes in COM energetics occurred. Our results suggest that these small changes in COM power were accompanied by negligible changes in COM dynamics but were instead driven by altered COM motion. However, maintaining COM dynamics with varying ankle exoskeleton properties requires modulating joint or muscle-level (*i.e.,* execution-level) dynamics [5, 7, 36, 43]. Therefore, quantifying subject-specific trade-offs between the modulation of task-level and execution level dynamics may improve our understanding of responses to exoskeletons or other assistive devices.

Conversely, in one stroke survivor, ankle exoskeletons impacted COM dynamics. The addition of exoskeleton mass and frame (K_0) increased paretic limb sagittal-plane rotary stiffness in first double-limb support and leg stiffness in single-limb and second double-limb support. Increased paretic-leg stiffness is

likely due to the exoskeleton frame restricting ankle inversion, which the participant noted during data collection. As the participant's paretic ankle was severely affected, restricting frontal-plane ankle motion may have increased leg stiffness by stabilizing the ankle. This result emphasizes the importance of quantifying the impacts of ankle exoskeleton properties beyond flexion stiffness, such as restriction to frontal-plane ankle motion, in explaining exoskeleton impacts on gait following neurological injury [1, 5, 44].

The insensitivity of the paretic limb template signatures to exoskeleton stiffness during single-limb support suggests that for this individual exoskeleton stiffness did not alter body weight support strategies [45]. As the zero-stiffness exoskeletons increased leg stiffness, it is possible that resisting frontal-plane ankle motion was the primary driver of changes in overall leg stiffness. That is, exoskeleton dorsiflexion stiffness did not further increase the paretic ankle's contribution to body-weight support. Conversely, during double-limb support, paretic-leg rotary stiffness increased compared to the zero-stiffness exoskeleton condition. This change in COM dynamics suggests that exoskeletons primarily altered dynamics impacting forcing transverse to the leg, which primarily contribute to propulsion and stabilization [46]. Unlike single-limb support, exoskeleton stiffness in terminal stance may enable increased propulsive force in the paretic limb, potentially explaining rotary mechanisms' increased contributions to gait. Further, the ankle plantarflexors accelerate the COM laterally, such that increased paretic plantarflexion torque capacity may impact frontal-plane dynamics as well [47, 48]. Note that, while these results indicate that our participant's task-level dynamics corresponding to stabilization and propulsion were impacted by exoskeleton stiffness, this result is likely to differ between stroke survivors [2]. Specifically, exoskeleton impacts on COM dynamics may depend on an individual's ability to convert exoskeleton assistance into functionally relevant forcing. While limited to a case study, our results highlight the potential contributions of ankle exoskeleton frame and stiffness on post-stroke COM dynamics that can be described by template signatures.

Template signatures quantify inter-individual and inter-limb differences in COM dynamics

Both unimpaired and post-stroke template signatures highlighted inter-individual and inter-limb differences in COM dynamics. While SLIP mechanisms described COM dynamics in all unimpaired limbs, rotary mechanisms were selected in only 50% of limbs during double-limb support. The uniform selection of SLIP mechanisms from data is consistent with common template walking models and supports the common perspective that elastic legs are foundational mechanisms for describing COM accelerations during walking across individuals [13, 21, 22, 26, 49]. Our observation that rotary mechanisms were not critical to reconstructing COM accelerations for all individuals may explain their less frequent application in template walking models [14, 20]. Note that each template signature mechanism describes characteristic coordination patterns between leg kinematics and COM accelerations. It is possible SLIP mechanisms describe coordination patterns necessary for stable or efficient walking, while rotary mechanisms describe coordination patterns that have smaller, more individualized impacts on gait. Determining which individual-specific characteristic patterns are predictive of exoskeleton responses or walking function represents important areas of future research.

Template signatures also revealed compensation strategies in one stroke survivor. Consistent with template-based studies in children with cerebral palsy, the stroke participant's paretic leg was stiffer than the nonparetic leg in single- and second double-limb support [29, 30]. Increased paretic leg stiffness may reflect a more pendular gait post-stroke and increased paretic-leg co-contraction [50]. In first double-limb support, sagittal-plane rotary stiffness and damping suggest altered braking dynamics during loading response. This possibility is consistent with experimental observations that the paretic-leg does greater negative work than the non-paretic limb during loading response in individuals post-stroke [12]. These results highlight the functional interpretability of data-driven template signatures and the importance of

476 personalized parameterizations of COM dynamics for elucidating inter-limb differences in COM
477 dynamics.
478

479 ## Innovation of Hybrid-SINDy for quantifying human gait

480 Our use of the Hybrid-SINDy algorithm ([33, 34]) was essential to elucidating individual-specific and
481 limb-specific changes in COM dynamics with ankle exoskeletons. By automatically identifying and
482 selecting different first principles-based representations of COM dynamics, we rapidly compared
483 competing hypotheses about human gait dynamics. Conversely, manually comparing all possible template
484 signatures for our fourteen-dimensional mechanism library would require a combinatorially-large number
485 of models to be generated, fit, and compared. Using a principled approach to model identification and
486 selection, Hybrid-SINDy selected dynamics that are consistent with literature in a fraction of the time
487 required to manually compare each candidate model.
488

489 To our knowledge, only one other study in bipedal locomotion has taken a similar approach [51]. The
490 authors performed a multi-layer optimization to select human-like template dynamics for walking robot
491 controllers. Our approach extends their work by using information criteria to enable multiple highly-
492 plausible representations of walking dynamics to be selected and analyzed for an individual [35, 40]. For
493 most participants, the Hybrid-SINDy algorithm selected a unique template signature, indicating that
494 alternative hypothetical representations of COM dynamics lacked strong statistical support. By
495 identifying multiple plausible template signatures for an individual, future experiments may be designed
496 to better differentiate between plausible signatures. To our knowledge, this work is the first to apply
497 Hybrid-SINDy to real data and the first to apply it to human gait.
498

499 Since reduced-order models are often sensitive to measurement noise and inevitably incorrect model
500 dynamics, we used a simulated SLIP with known dynamics to evaluate the extent to which Hybrid-

SINDy correctly identified template signatures during walking. Hybrid-SINDy performed as expected in the noise-free condition, accurately identifying single-limb support and swing dynamics, except for small damping terms. Terms with small contributions to system behavior, such as damping in this study, may be omitted by the AICc in favor of parsimony [35, 40]. An important implication of this result is that our approach will not always select the true system dynamics but will select terms critical to describing salient behavior of the system. Therefore, designing experimental protocols capable of probing candidate mechanisms is critical to accurately identifying walking dynamics from data. For example, gait patterns that induced large leg velocities may result in damping terms having a larger impact on COM dynamics and being correctly selected by Hybrid-SINDy. Additionally, reduced simulated SLIP template signature accuracy in double-limb support and with increasing noise magnitude highlights the importance of collecting long time-series datasets to ensure that clusters are small enough to span only a single hybrid regime but large enough to remain robust to sensor noise [33].

Challenges and limitations

This study's limitations motivate future developments for data-driven modeling of human locomotion. First, human gait dynamics are continuously phase-varying rather than hybrid, such that template signature parameters varied continuously across clusters. However, preliminary analyses found candidate models' abilities to reconstruct COM dynamics diverged near the transitions between single and double-limb support, suggesting that changes in dynamics between foot contact configurations are larger than changes within configurations. Consequently, pre-defining hybrid regimes based on contact configuration was both appropriate and consistent with existing hybrid template models of walking [20, 21, 26, 33]. Second, we evaluated only a subset of mechanisms describing COM dynamics, which may not encode all important features of human gait. However, we chose a broad class of physically-meaningful mechanisms from literature ([18, 20-22, 26, 28]) that should motivate future studies using larger mechanism libraries describing COM dynamics. For example, our approach may be extended to include elements describing

assistive devices or joint-level mechanisms. Finally, our limited sample size may have masked exoskeleton impacts on unimpaired gait. Particularly, rotary stiffness appeared to increase slightly with exoskeletons but did not reach significance. Similarly, our post-stroke case study only provides a proof of concept highlighting the potential of ankle exoskeletons to elicit changes in COM dynamics. Evaluating template signatures on larger unimpaired and post-stroke cohorts may provide additional insight into how COM dynamics change with ankle exoskeletons.

Extensions and applications

Integrating principles from biomechanics and neuromechanics with state-of-the-art *interpretable* data-driven modeling techniques may accelerate discovery in mechanisms underlying diverse movement patterns in human locomotion. Broadly, these methods may be applied to any intervention or walking condition and may inform the design of prosthetic limbs and other assistive devices. A natural extension of this work is to investigate the impacts of powered exoskeletons on COM dynamics. Changes in gait kinematics and kinetics with our passive ankle exoskeletons were small compared to those elicited by powered exoskeletons, which may elicit larger changes in COM dynamics [2, 6, 36]. As powered exoskeleton research shifts its focus from reducing metabolic demand to assisting other locomotion objectives, such as stability or agility, understanding changes in COM dynamics with exoskeletons may provide insight into how individuals leverage exoskeletons to realize these goals [52]. Particularly in a clinical context, quantifying changes in COM dynamics with exoskeletons may improve our understanding of the diverse responses to exoskeletons observed in individuals with neurological injuries [1-3]. For example, McCain and colleagues (2019) identified limb orientation as a potential mechanism impacting the conversion of exoskeleton torque to forward propulsion post-stroke [2]. Our results in one stroke survivor suggest that characterizing altered coordination between leg orientation and ground reaction forces (*i.e.,* template signatures) may unveil sub-classes of exoskeleton responses, enabling device customization to assist individuals in each sub-class. Finally, using similar physics-informed data-

551 driven approaches to *anchoring* template signatures in physiological detail may reveal biological
552 mechanisms that characterize responses to exoskeletons or other assistive devices [14, 16].
553

554 ## Conclusions

555 We quantified changes in subject-specific COM dynamics in response to passive ankle exoskeletons
556 using a novel physics-informed data-driven modeling framework, Hybrid-SINDy. Hybrid-SINDy
557 successfully constructed characteristic template signatures during walking by identifying salient
558 mechanisms describing an individual's COM accelerations. Unimpaired adults maintained nearly
559 invariant COM dynamics with ankle exoskeletons, while exoskeletons altered COM dynamics in an
560 individual post-stroke. These findings provide insight into task-level control of walking dynamics with
561 ankle exoskeletons and extend a powerful data-driven modeling tool to human locomotion.
562
563

564 ## Acknowledgements

565 This material is based upon work supported by the National Science Foundation under grant no. CBET-
566 1452646 to KMS, the National Science Foundation Graduate Research Fellowship Program under grant
567 no. DGE-1762114 to MCR, and a University of Washington Gatzert Child Welfare Fellowship to MCR.

References

[1] Kerkum, Y.L., Buizer, A.I., van den Noort, J.C., Becher, J.G., Harlaar, J. & Brehm, M.-A. 2015 The effects of varying ankle foot orthosis stiffness on gait in children with spastic cerebral palsy who walk with excessive knee flexion. *PloS one* **10**, e0142878.

[2] McCain, E.M., Dick, T.J., Giest, T.N., Nuckols, R.W., Lewek, M.D., Saul, K.R. & Sawicki, G.S. 2019 Mechanics and energetics of post-stroke walking aided by a powered ankle exoskeleton with speed-adaptive myoelectric control. *Journal of neuroengineering and rehabilitation* **16**, 1-12.

[3] Ries, A.J., Novacheck, T.F. & Schwartz, M.H. 2015 The efficacy of ankle-foot orthoses on improving the gait of children with diplegic cerebral palsy: a multiple outcome analysis. *PM&R* **7**, 922-929.

[4] Lerner, Z.F., Harvey, T.A. & Lawson, J.L. 2019 A Battery-Powered Ankle Exoskeleton Improves Gait Mechanics in a Feasibility Study of Individuals with Cerebral Palsy. *Annals of biomedical engineering* **47**, 1345-1356.

[5] Collins, S.H., Wiggin, M.B. & Sawicki, G.S. 2015 Reducing the energy cost of human walking using an unpowered exoskeleton. *Nature* **522**, 212-215.

[6] Jackson, R.W., Dembia, C.L., Delp, S.L. & Collins, S.H. 2017 Muscle–tendon mechanics explain unexpected effects of exoskeleton assistance on metabolic rate during walking. *Journal of Experimental Biology* **220**, 2082-2095.

[7] Sawicki, G.S. & Khan, N.S. 2016 A Simple Model to Estimate Plantarflexor Muscle–Tendon Mechanics and Energetics During Walking With Elastic Ankle Exoskeletons. *IEEE Transactions on Biomedical Engineering* **63**, 914-923.

[8] Jackson, R.W. & Collins, S.H. 2015 An experimental comparison of the relative benefits of work and torque assistance in ankle exoskeletons. *Journal of applied physiology* **119**, 541-557.

[9] Donelan, J.M., Kram, R. & Kuo, A.D. 2002 Mechanical work for step-to-step transitions is a major determinant of the metabolic cost of human walking. *Journal of Experimental Biology* **205**, 3717-3727.

592 [10] Kuo, A.D. 1999 Stabilization of Lateral Motion in Passive Dynamic Walking. *The International*
593 *Journal of Robotics Research* **18**, 917-930. (doi:10.1177/02783649922066655).
594 [11] Kuo, A.D. 2007 The six determinants of gait and the inverted pendulum analogy: A dynamic
595 walking perspective. *Human movement science* **26**, 617-656.
596 [12] Farris, D.J., Hampton, A., Lewek, M.D. & Sawicki, G.S. 2015 Revisiting the mechanics and
597 energetics of walking in individuals with chronic hemiparesis following stroke: from individual limbs to
598 lower limb joints. *Journal of neuroengineering and rehabilitation* **12**, 1-12.
599 [13] Alexander, R.M. 1995 Simple models of human movement.
600 [14] Davoodi, A., Mohseni, O., Seyfarth, A. & Sharbafi, M.A. 2019 From template to anchors: transfer of
601 virtual pendulum posture control balance template to adaptive neuromuscular gait model increases
602 walking stability. *Royal Society open science* **6**, 181911.
603 [15] McGeer, T. 1990 Passive dynamic walking. *I. J. Robotic Res.* **9**, 62-82.
604 [16] Full, R.J. & Koditschek, D.E. 1999 Templates and anchors: neuromechanical hypotheses of legged
605 locomotion on land. *Journal of experimental biology* **202**, 3325-3332.
606 [17] Cavagna, G.A., Heglund, N.C. & Taylor, C.R. 1977 Mechanical work in terrestrial locomotion: two
607 basic mechanisms for minimizing energy expenditure. *American Journal of Physiology-Regulatory,*
608 *Integrative and Comparative Physiology* **233**, R243-R261.
609 [18] Holmes, P., Full, R.J., Koditschek, D. & Guckenheimer, J. 2006 The dynamics of legged
610 locomotion: Models, analyses, and challenges. *SIAM review* **48**, 207-304.
611 [19] Srinivasan, M. & Ruina, A. 2006 Computer optimization of a minimal biped model discovers
612 walking and running. *Nature* **439**, 72.
613 [20] Antoniak, G., Biswas, T., Cortes, N., Sikdar, S., Chun, C. & Bhandawat, V. 2019 Spring-loaded
614 inverted pendulum goes through two contraction-extension cycles during the single-support phase of
615 walking. *Biology open* **8**.

[21] Lipfert, S.W., Günther, M., Renjewski, D., Grimmer, S. & Seyfarth, A. 2012 A model-experiment comparison of system dynamics for human walking and running. *Journal of theoretical biology* **292**, 11-17.

[22] Maus, H.-M., Lipfert, S., Gross, M., Rummel, J. & Seyfarth, A. 2010 Upright human gait did not provide a major mechanical challenge for our ancestors. *Nature communications* **1**, 1-6.

[23] Garcia, M., Chatterjee, A., Ruina, A. & Coleman, M. 1998 The simplest walking model: stability, complexity, and scaling.

[24] Buczek, F.L., Cooney, K.M., Walker, M.R., Rainbow, M.J., Concha, M.C. & Sanders, J.O. 2006 Performance of an inverted pendulum model directly applied to normal human gait. *Clinical Biomechanics* **21**, 288-296.

[25] Donelan, J.M., Shipman, D.W., Kram, R. & Kuo, A.D. 2004 Mechanical and metabolic requirements for active lateral stabilization in human walking. *Journal of biomechanics* **37**, 827-835.

[26] Geyer, H., Seyfarth, A. & Blickhan, R. 2006 Compliant leg behaviour explains basic dynamics of walking and running. *Proceedings of the Royal Society B: Biological Sciences* **273**, 2861-2867.

[27] Dingwell, J.B. & Cusumano, J.P. 2019 Humans use multi-objective control to regulate lateral foot placement when walking. *PLoS computational biology* **15**, e1006850.

[28] Kim, S. & Park, S. 2011 Leg stiffness increases with speed to modulate gait frequency and propulsion energy. *Journal of Biomechanics* **44**, 1253-1258. (doi:https://doi.org/10.1016/j.jbiomech.2011.02.072).

[29] Holt, K.G., Fonseca, S.T. & LaFiandra, M.E. 2000 The dynamics of gait in children with spastic hemiplegic cerebral palsy: theoretical and clinical implications. *Human Movement Science* **19**, 375-405.

[30] Fonseca, S.r.T., Holt, K.G., Fetters, L. & Saltzman, E. 2004 Dynamic resources used in ambulation by children with spastic hemiplegic cerebral palsy: relationship to kinematics, energetics, and asymmetries. *Physical Therapy* **84**, 344-354.

[31] Brunton, S.L., Proctor, J.L. & Kutz, J.N. 2016 Discovering governing equations from data by sparse identification of nonlinear dynamical systems. *Proceedings of the National Academy of Sciences* **113**, 3932-3937.

[32] Brunton, S.L. & Kutz, J.N. 2019 *Data-driven science and engineering: Machine learning, dynamical systems, and control*, Cambridge University Press.

[33] Mangan, N.M., Askham, T., Brunton, S.L., Kutz, J.N. & Proctor, J.L. 2019 Model selection for hybrid dynamical systems via sparse regression. *Proceedings of the Royal Society A* **475**, 20180534.

[34] Mangan, N.M., Kutz, J.N., Brunton, S.L. & Proctor, J.L. 2017 Model selection for dynamical systems via sparse regression and information criteria. *Proceedings of the Royal Society A: Mathematical, Physical and Engineering Sciences* **473**, 20170009.

[35] Anderson, D. & Burnham, K. 2004 Model selection and multi-model inference. *Second. NY: Springer-Verlag* **63**.

[36] Rosenberg, M.C., Banjanin, B.S., Burden, S.A. & Steele, K.M. 2020 Predicting walking response to ankle exoskeletons using data-driven models. *Journal of the Royal Society Interface* **17**, 20200487.

[37] Genthe, K., Schenck, C., Eicholtz, S., Zajac-Cox, L., Wolf, S. & Kesar, T.M. 2018 Effects of real-time gait biofeedback on paretic propulsion and gait biomechanics in individuals post-stroke. *Topics in stroke rehabilitation* **25**, 186-193.

[38] Delp, S.L., Anderson, F.C., Arnold, A.S., Loan, P., Habib, A., John, C.T., Guendelman, E. & Thelen, D.G. 2007 OpenSim: open-source software to create and analyze dynamic simulations of movement. *IEEE transactions on biomedical engineering* **54**, 1940-1950.

[39] Rajagopal, A., Dembia, C.L., DeMers, M.S., Delp, D.D., Hicks, J.L. & Delp, S.L. 2016 Full-body musculoskeletal model for muscle-driven simulation of human gait. *IEEE transactions on biomedical engineering* **63**, 2068-2079.

[40] Akaike, H. 1974 A new look at the statistical model identification. In *Selected Papers of Hirotugu Akaike* (pp. 215-222, Springer.

[41] Lee, C.R. & Farley, C.T. 1998 Determinants of the center of mass trajectory in human walking and running. *Journal of experimental biology* **201**, 2935-2944.

[42] Glantz, S. 2012 Primer of Biostatistics, 7th edn, pp. 65–67. (New York: McGraw-Hill.

[43] Steele, K.M., Jackson, R.W., Shuman, B.R. & Collins, S.H. 2017 Muscle recruitment and coordination with an ankle exoskeleton. *Journal of biomechanics* **59**, 50-58.

[44] Hegarty, A.K., Petrella, A.J., Kurz, M.J. & Silverman, A.K. 2016 Evaluating the Effects of Ankle Foot Orthosis Mechanical Property Assumptions on Gait Simulation Muscle Force Results. *Journal of Biomechanical Engineering*.

[45] Neptune, R.R., Clark, D.J. & Kautz, S.A. 2009 Modular control of human walking: a simulation study. *Journal of biomechanics* **42**, 1282-1287.

[46] Neptune, R.R., Kautz, S.A. & Zajac, F.E. 2001 Contributions of the individual ankle plantar flexors to support, forward progression and swing initiation during walking. *Journal of biomechanics* **34**, 1387-1398.

[47] Pandy, M.G., Lin, Y.-C. & Kim, H.J. 2010 Muscle coordination of mediolateral balance in normal walking. *Journal of Biomechanics* **43**, 2055-2064. (doi:http://dx.doi.org/10.1016/j.jbiomech.2010.04.010).

[48] Kim, M. & Collins, S.H. 2013 Stabilization of a three-dimensional limit cycle walking model through step-to-step ankle control. In *Rehabilitation Robotics (ICORR), 2013 IEEE International Conference on* (pp. 1-6, IEEE.

[49] Mochon, S. & McMahon, T.A. 1980 Ballistic walking. *Journal of biomechanics* **13**, 49-57.

[50] Clark, D.J., Ting, L.H., Zajac, F.E., Neptune, R.R. & Kautz, S.A. 2010 Merging of Healthy Motor Modules Predicts Reduced Locomotor Performance and Muscle Coordination Complexity Post-Stroke. *Journal of Neurophysiology* **103**, 844-857. (doi:10.1152/jn.00825.2009).

[51] Chen, Y.-M. & Posa, M. 2020 Optimal reduced-order modeling of bipedal locomotion. In *2020 IEEE International Conference on Robotics and Automation (ICRA)* (pp. 8753-8760, IEEE.

690 [52] Sawicki, G.S., Beck, O.N., Kang, I. & Young, A.J. 2020 The exoskeleton expansion: improving
691 walking and running economy. *Journal of NeuroEngineering and Rehabilitation* **17**, 25.
692 (doi:10.1186/s12984-020-00663-9).
693